Hindawi
International Journal of Geophysics
Volume 2018, Article ID 9434251, 12 pages
https://doi.org/10.1155/2018/9434251

Research Article

Geomorphology Characterization of Ica Basin and Its Influence on the Dynamic Response of Soils for Urban Seismic Hazards in Ica, Peru

Isabel Bernal, Hernando Tavera, Wilfredo Sulla, Luz Arredondo, and Javier Oyola

Instituto Geofísico del Perú (IGP), Lima, Peru

Correspondence should be addressed to Isabel Bernal; ybernal@igp.gob.pe

Received 16 June 2017; Accepted 27 November 2017; Published 17 January 2018

Academic Editor: Rudolf A. Treumann

We evaluated the influence of the geomorphology of Peru's Ica Basin on the dynamic response of soils of the city of Ica. We applied five geophysical methods: spectral ratio (H/V), frequency-wavenumber (F-K), multichannel analysis of surface waves (MASW), multichannel analysis of microtremor (MAM), and Gravimetric Analysis. Our results indicate that the soils respond to two frequency ranges: $F0$ (0.4–0.8 Hz) and $F1$ (1.0–3.0 Hz). The F-K, which considers circular arrays, shows two tendencies with a jump between 1.0 and 2.0 Hz. MASW and MAM contribute to frequencies greater than 2.0 Hz. The inversion curve indicates the presence of three layers of 4, 16, and 60 m with velocities of 180, 250, and 400 m/s. The Bouguer anomalies vary between −17.72 and −24.32 mGal and with the spectral analysis we identified two deposits, of 60 m and 150 m of thickness. Likewise, the relationship between the velocities of 400 and 900 m/s, with the frequency = 1.5 Hz, allows us to determine the thickness for the layers of 60 (slightly alluvial to moderately compact) and 150 m (soil-rock interface). These results suggest that the morphology of the Ica Basin plays an important role in the dynamic behavior of the soils to low frequency.

1. Introduction

Ica Basin (IB) is a depression located in western central Peru between the Coastal and Western Andean mountains (Figure 1). In lower basin is located the urban area of Ica city. The main geodynamic events affecting Ica are earthquakes, inundations, debris flows, rock falls, and sandy eolic deposit.

Ica has been severely damaged by earthquakes, such as the quakes in 1942 (7.8 Mw) and 1996 (7.6 Mw) and most recently the 8.0 Mw Pisco earthquake of 2007. The Pisco earthquake generated maximum intensities of VII-VIII on the Modified Mercalli Intensity Scale within a 250 km radio, including the cities Pisco, Ica, and Chincha. This was one of the largest earthquake of the last 300 years [1] and showed particular characteristics such as its duration (120 s) and a complex rupture process that induced a local tsunami. The most significant structural damage was observed in adobe and "quincha" houses, which resulted in more than 590 fatalities and 320 injuries [2]. The structural damage observed in more than 12 villages around Ica, Lima, and Huancavelica was mainly associated with local site effects (i.e., soil liquefaction along the coastline and in weakly consolidated soils), the age of structures, and landslides on the roads [3]. The study area is located on thick alluvial deposits composed of pebbles and small blocks embedded in a silty sand matrix [4]. This soil type and quality will contribute to generating damage on the surface when earthquake occurs; therefore, it is necessary to determine the sedimentary basin's geometry to better understand its dynamic behavior [5]. Understanding this depends on the soil and basin's physical and geomechanical properties (e.g., stratigraphy, lithology, layer thickness, and basal rock), because they control propagation velocity of shear waves (Vs).

In this study, we evaluate the influence of the geomorphology characterization of the Ica Basin and the dynamic response of soils for urban seismic hazards in Ica. To estimate these characteristics, we applied five geophysical methods: spectral ratio (H/V), frequency-wavenumber (F-K), multichannel analysis of surface waves (MASW), multichannel analysis of microtremor (MAM), and gravimetric method. We then used these results to know the seismic and

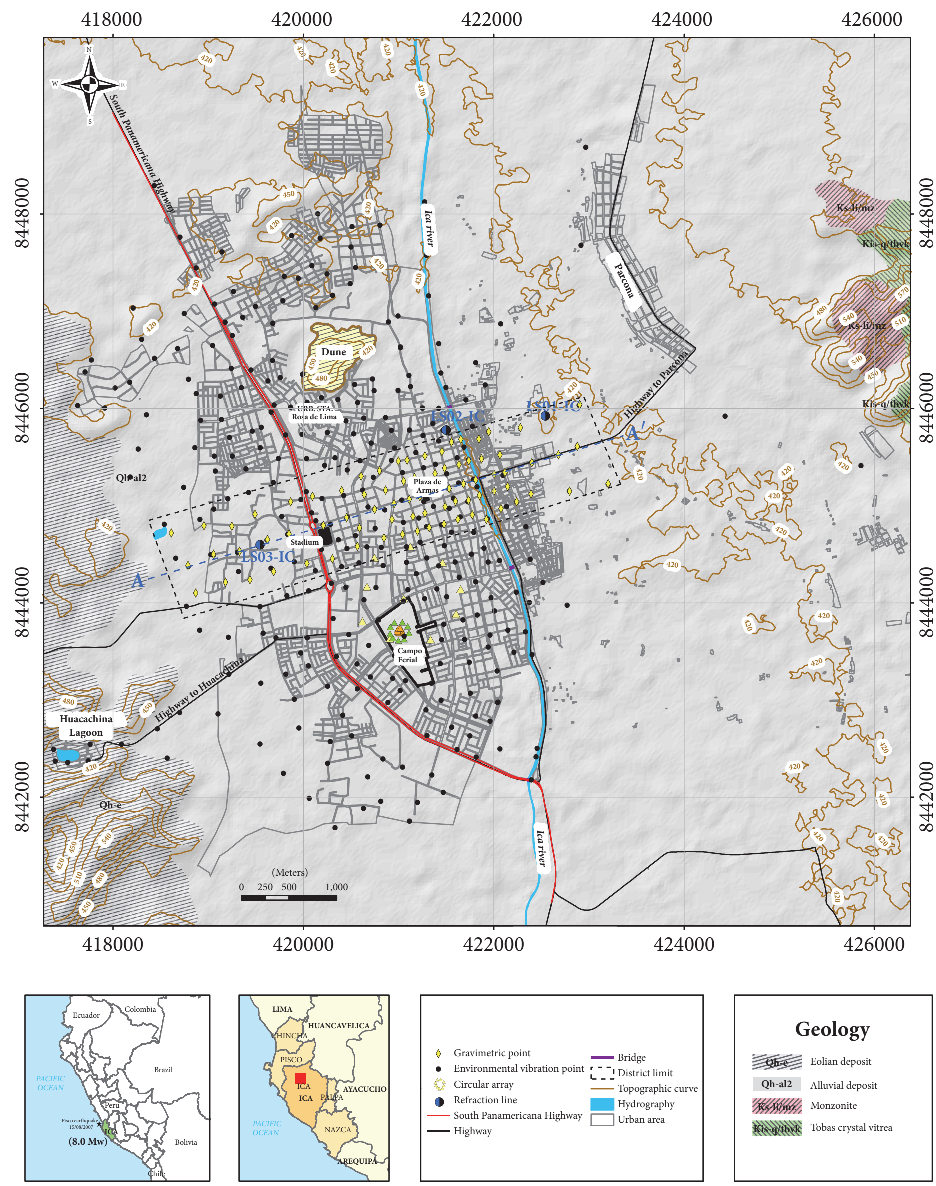

Figure 1: Geological setting of Ica, Peru. Black dots correspond to the locations of environmental vibration record, yellow diamonds correspond to gravimetric measurements, and yellow and green triangles correspond to circular seismic arrays. The LS01–LS03 line represents the linear seismic array. The A-A′ labels indicate the orientation of the gravimetric profile.

geophysical properties of soils of Ica city and generate a two-dimensional (2D) model of the Ica Basin.

1.1. Geological Framework. The city of Ica represents 36% of the total surface of the Ica Department and is located in the lower part of the Ica River Basin (Figure 1). According to Gomez et al. [6], the most representative geomorphological features in the area are the dunes, which are formed by coastal winds near the shoreline and the plain or alluvial valley the city sits on. The rocky basement of this region is characterized by a Precambrian coastal basal complex composed of metamorphic rocks and in surface by quaternary deposits. The soils in this area consist of sands and silty-sands with some fine contents. From a geotechnical perspective, Ica's urban area is characterized by soils with low bearing capacity (1.0–2.0 kg/cm^2), although some areas toward the southwest and southeast show very low (<1.0 kg/cm^2) and medium (2.0–3.0 kg/cm^2) bearing capacities, respectively.

2. Methods

2.1. Description of the Methods. In order to know the influence of the geomorphology of the Ica Basin on the dynamic response of soils for urban in Ica, we applied five geophysical methods: spectral ratio (H/V), frequency-wavenumber (F-K), multichannel analysis of surface waves (MASW), multichannel analysis of microtremor (MAM), and gravimetric method.

2.2. Spectral Ratio (H/V) Method. This method allows calculating the empirical soil transfer function (FTE) from the spectral ratio of the horizontal and vertical component of an environmental vibration record (natural noise and/or noise generated by human activity) considering that the vertical component is not affected by the sedimentary deposits [7–10]. These spectra allow us to know the dynamic parameters of the soil such as the fundamental frequency, the dominant period, and the maximum relative amplifications of the soil. Nakamura [11] reaffirms that the spectral quotient is a reliable estimate of the site transfer function for *S* waves, allowing identification of the fundamental frequency of resonance of sedimentary deposits [12, 13].

2.3. Frequency-Wavenumber (F-K) Method. This method allows obtaining the velocity profile of the shear waves (Vs) and thickness of sedimentary deposits. This method considers that the array of sensors is traversed by a flat-wave front [14, 15] of known frequency, velocity, and direction of propagation, given in a two-dimensional space defined by the wavenumber in the direction of Kx, Ky [16], Socco et al. 2010. Finally, the transformation frequency number of wave frequency F-K [14, 17, 18] allows obtaining the dispersion curve to determine the phase velocity of Rayleigh waves according to their vibration mode [19, 20]. The fundamental vibration mode is characterized by attenuation in amplitude as the depth increases and the superior modes (first-mode, second-mode, etc.) by presenting varying amplitudes at different depth levels [21–24]. Likewise, the nature of the higher modes results from the constructive interference of wave reflection in the Earth's crust [25–27], Foti et al. 2014.

For F-k, the most sensitive parameters are associated with the reliability range of each seismic array (Figure 2(a)) because they depend on distance (D), wavelength (λ), and number of waves (K), where Kmin and Kmax, given in a two-dimensional space Kx and Ky (Figures 2(b) and 2(c)), define the greatest and least contribution of energy to propagating waves. In Figure 2(d), the discontinuous curves sectorize the dispersion curves and delimit the highest resolution zones for the dispersion curve, identifying low energy zones (lower frequency values) and aliasing zones with several energy peaks (greater frequency values). The first is associated with the boundary imposed by the width of the central lobe of the array's response function, while aliasing is associated with the minimum spacing between geophones.

For the inversion of the dispersion curve, the neighbourhood algorithm [28] is considered, which makes use of Voronoi's cell decomposition of the spatial parameters, based on an approximation of the "misfit" function, which is progressively refined during the inversion process. The misfit is proportional to the error in the adjustment of the empirical dispersion curve with the theoretical curve obtained with the proposed velocity profile. This parameter must tend toward low values. For this approach, more than 500 speed models are generated to consider a misfit less than 0.2. The misfit function is defined by the following equation [29]:

$$\text{misfit} = \sqrt{\sum_{i=1}^{n_F} \frac{\left(x_{di} - x_{ci}\right)^2}{\sigma_i^2 n_F}}, \tag{1}$$

where x_{di} is the velocity of the frequency curve f_i, x_{ci} is the velocity of the calculated curve at the frequency curve f_i, σ_i^2 is the uncertainty of the frequency sample, and n_F is the sample frequency number. Finally, the dispersion curve with its different modes, through a nonlinear process, is inverted in order to look for a theoretical profile that fits this experimental dispersion curve.

In order to validate the results, the velocity models (Vs) obtained through this process were inverted to obtain a theoretical transfer function (FTT) by applying the Thomson-Haskell method for horizontal stratified media subject to SH wave action [20, 30], to finally overlay the FTT with the empirical transfer function (FTE).

2.4. MASW and MAM Methods. Both methods make it possible to determine the one-dimensional seismic profile of waves (Vs) by means of surface wave measurement tests, the resolution of which differs at surface and deep levels, respectively. Multichannel arrays of sensors located at predetermined distances along an axis along the ground surface are considered. MASW considers waves generated by an impulsive energy source at predetermined points and MAM considers the recording of environmental vibrations. From these methods we obtain dispersion curves of Rayleigh waves (phase velocity of the superficial waves versus frequency) and their inversion allows us to determine the profile of *S* wave velocity (Vs) [31, 32], Socco et al., 2010.

2.5. Gravimetric Method. This method allows the depth of the soil-rock interface to be determined from the variation of gravity acceleration on the ground. The method detects variations in densities in geological units present in the subsoil (density > 2 gm/cm3 is associated with rocks and lower with sediments).

The gravimetric data were corrected by free-air using regional (Shuttle Radar Topographic Mission, SRTM) and local elevation models (50 × 50 meters' resolution grid). The Oasis Montaj software from Geosoft and an average rock density of 2.5 g/cm3 [33] were used to correct Bouguer. For topographic correction, the methodology proposed by Kane [34] and Nagy [35] is considered, in order to obtain a grid of topographic correction, which through a sampling operation assigns the correction value to each gravimetric point. Finally, the Bouguer anomaly values are triangular interpolated.

In order to estimate the depth of the anomalies, the spectral analysis method proposed by Spector (1968) and Grant (1970) is used, which allows the grid of Bouguer's anomaly to be transformed into the space domain and the frequency domain. The values corresponding to each slope of the spectrum, divided by 4π, allow knowing the average depth of the center of mass of each anomaly. The first line slope is associated with the depth of the masses generating the regional anomaly, the second with the depth of the intermediate sources, and the third with the more superficial sources.

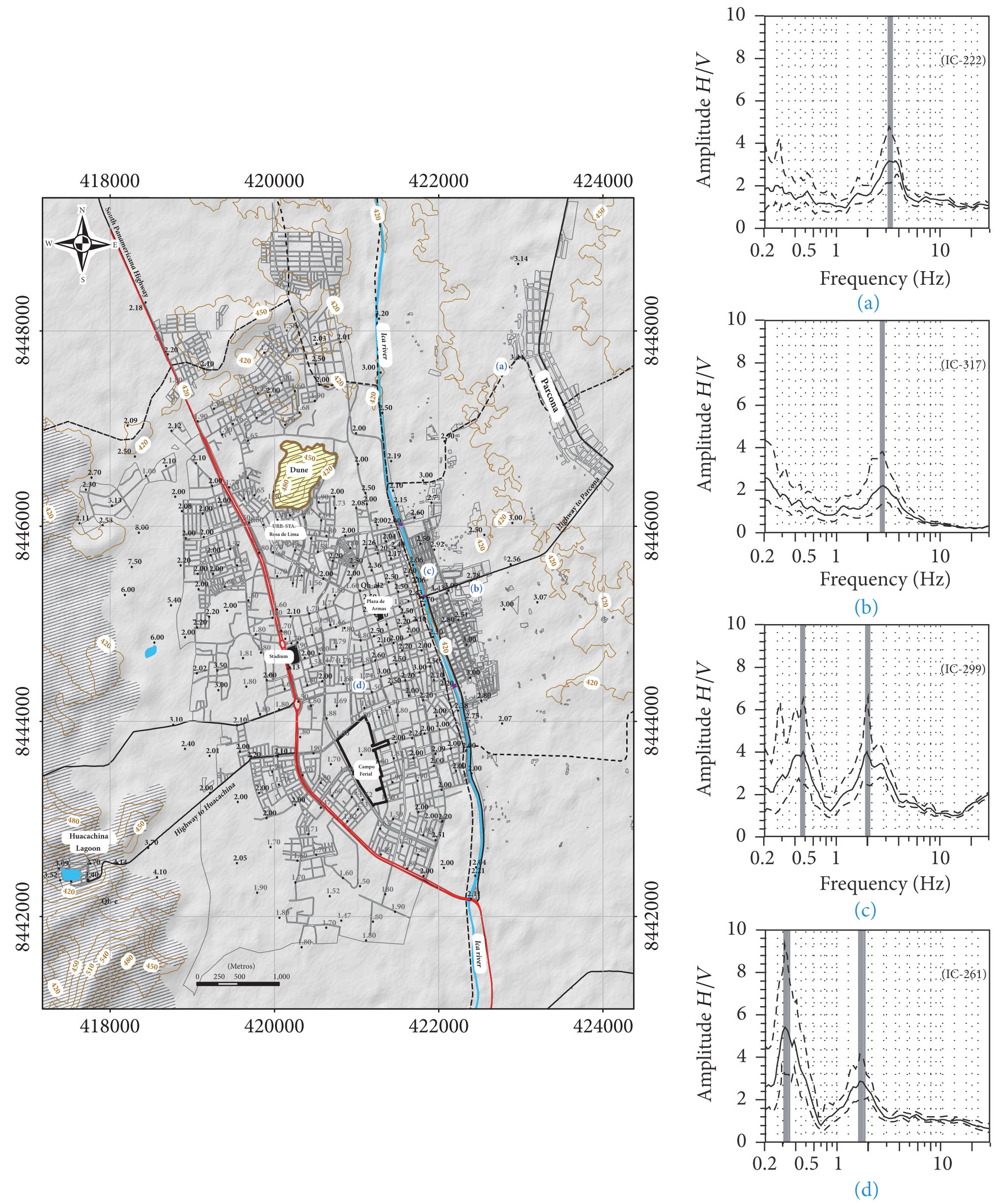

Figure 2: Spatial distribution of the frequency $F1$ ($F > 1.0$ Hz) and examples of spectral ratios obtained in several locations.

3. Data Acquisition

Figure 1 shows the locations of the individual measurement sites discussed in this study. To apply the H/V technique, we used microtremor data collected from 300 measurement points using a Lennartz LE-3D/5s seismometer and a CityShark digitizer, with a duration of 15 minutes per measuring point. To select which points to record, we considered the study area's geological and geomorphological characteristics, as well as the distribution of urban areas and accessibility. To apply the F-K method, we used microtremors data obtain by mean circular arrays of seismometers with 10, 30, 100, and 400 m radius, acquiring between approximately 30 minutes and 4 hours of data on each array, depending on its diameter. We considered the center of the arrays the "Campo Ferial of Ica." For these arrays we used 10 Guralp 3-channel seismometers, each with a 24-bit Reftek digitizer.

The MASW and MAM methods use linear arrays of geophones (sensors), located at predefined distances along an axis on the surface. The MASW method considers the waves generated by an impulsive energy source at predefined sites. In the MAM method, use environmental vibrations. Both methods allow us to obtain the dispersion curve of the surface waves (phase velocity versus frequency) and its inversion allows determining the S-waves velocity profile (Vs) [31, 32], Socco et al., 2010. For both methods, we used an ES-300 instrument equipped with 24 sensors, with a sensitivity of 4.5 Hz. We assembled three arrays 144 and 240 m long, in the center and the boundary of the Ica Basin. On the other hand, for gravimetric method, we performed 80 gravimetric

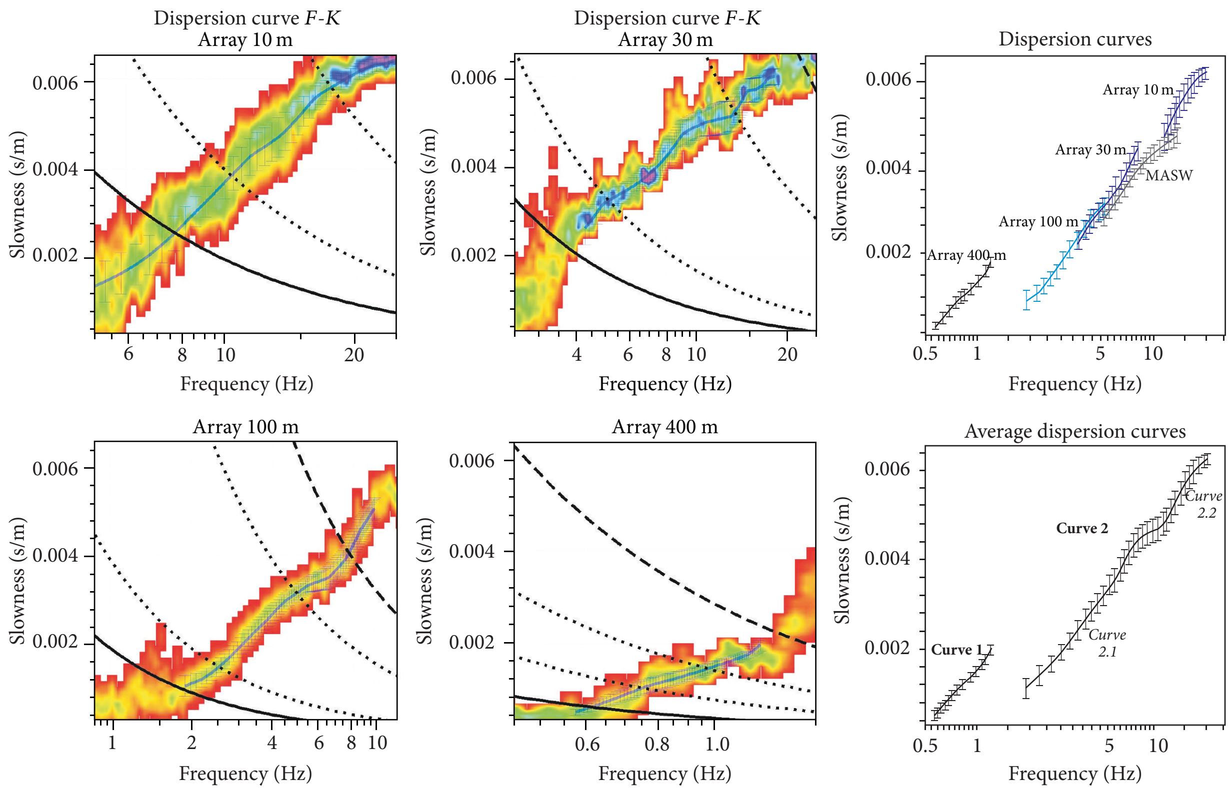

FIGURE 3: Dispersion curves (slowness versus frequency) obtained using the *F-K* method, which considers circular arrays with radii of 10, 30, 100, and 400 m. Dashed lines indicate reliability ranges and the bars in the curves are associated with the dispersion of slowness for each frequency. The right panels show the dispersion curves for different seismic arrays and the solid black line represents the average.

measurements distributed in five parallel lines (SW-NE), separated by an average distance of 300 m (Figure 1). The distance between each measurement is about 200 m. For the measurements we used a Lacoste & Romberg gravimeter with an accuracy of ±0.01 mGal. We applied an absolute gravity correction, using as reference base a point near the Rio Grande Tunnel (978215.134 mGal) south of Ica (Figure 1). The position of each site (coordinates and ellipsoidal elevation) used the WGS84 system and was determined using a Nikon DTM-322 Total Station.

4. Results

The predominant frequency (Fr), shear wave velocity (*Vs*) of the different soil layers, and the depth of the soil-rock interface are three important parameters in the characterization of physical and dynamic properties of soils to know the urban seismic hazards in Ica.

4.1. Predominant Frequency (Fr). The frequency analysis (Fr) shows that soil of Ica responds in two frequency ranges (Figure 2), $F0$ ($F < 1.0$ Hz) and $F1$ ($F > 1.0$ Hz), with amplifications varying from factors of 2 to 6 depending on the location. For $F0$ we observed Fr between 0.4 and 0.8 Hz, with relative amplifications up to a factor of 5. For $F1$, Frs lower than 2.0 Hz are distributed in the center of the Ica city and along the "Panamericana Sur" road. Toward the eastern and western borders of Ica, $F1$ showed higher frequencies with relative amplifications of up to a factor of 6. Likewise, near "Santa Rosa de Lima Urbanization" (to the north), the Ica River (to the east), and the Huacachina Lagoon (to the southwestern), we observe Frs for $F0$ of 0.35, 0.40, and 0.48 and 1.8, 2.6, and 3.0 for $F1$, respectively. It is evident that the central part of the basin shows low $F0$ and $F1$ values, increasing gradually toward the borders of the basin.

Figure 2 shows four representative spectral ratios curves labeled (a), (b), (c), and (d). (d), located in the central area, is characterized by the predominance of $F0$ (0.4 Hz) over $F1$ (2.0 Hz). In (c), which is close to the Ica River, $F0$ and $F1$ are similar, whereas, in (a) and (b), to the east of the Ica River, we observe predominant $F1$ values between 2.0 and 4.0 Hz. These results show that in Ica's urban area there are two Fr ranges, $F0$ and $F1$. Although $F0$ tends to disappear, $F1$ shows higher values as the distance from/to the east from the basin's center increases. With these results we can infer that the dynamic behavior of the soils in Ica changes because the soil-rock interface presents an irregular geomorphology.

4.2. Shear Wave Velocity (Vs)

4.2.1. 1D Profile Using the F-K Method. Figure 3 shows the tendencies of the dispersion curves obtained by different seismic arrays. The reliability ranges (dashed lines) delimit the areas of maximum resolution for the dispersion curve. In this case, for a radius of 10 m the frequency range is 10 to 15 Hz, for 30 m it is 5.0 to 8.0 Hz, for 100 m it is 2.5 to 4.5 Hz, and for 400 m it is 0.8 to 1.5 Hz. We observe that the energy between the curves varies strongly between 1 and 2 Hz,

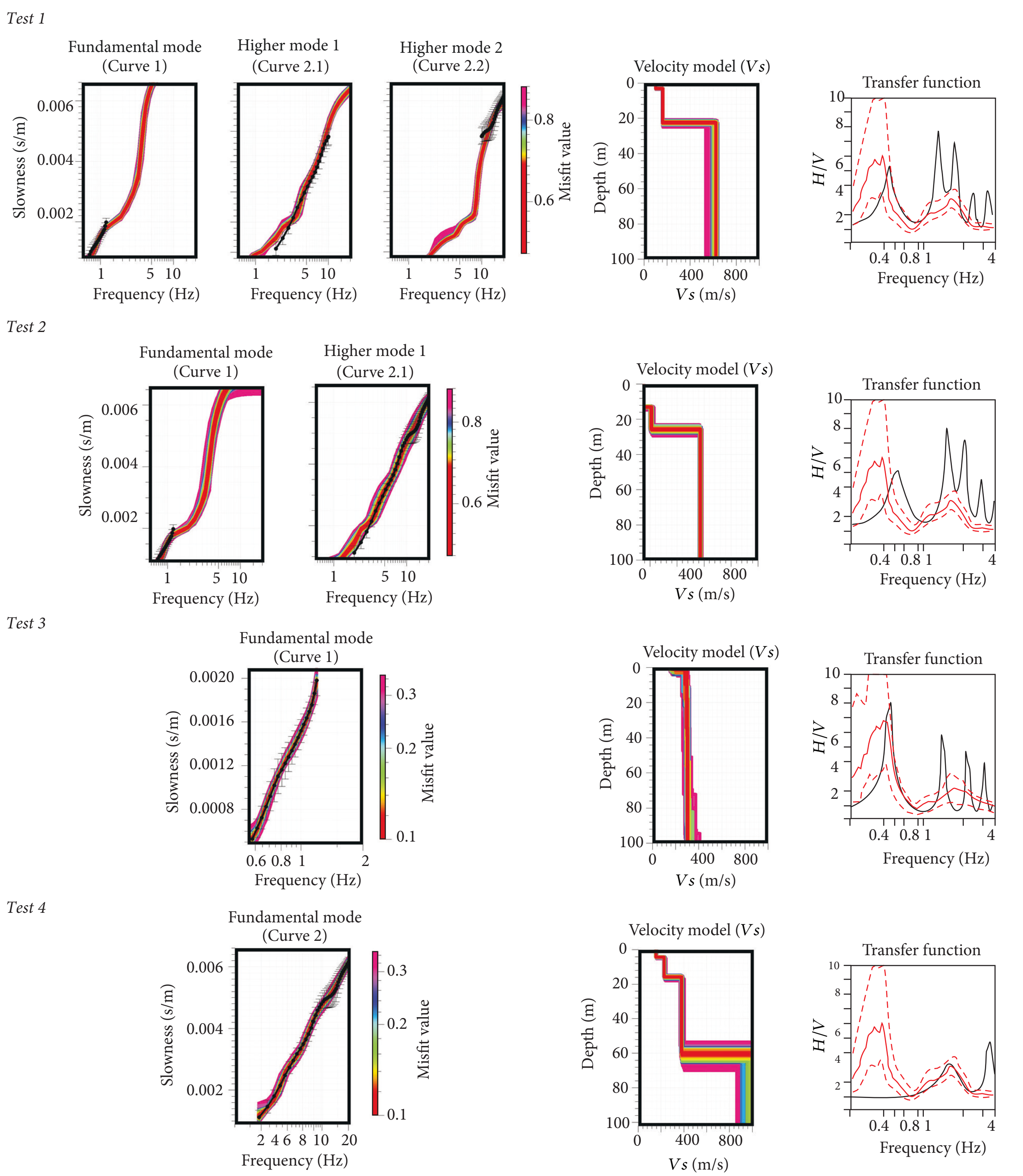

Figure 4: Results for the four tests, from left to right: the inversion of the dispersion curves, the velocity profiles of shear waves (*Vs*), and the correspondence of the theoretical transfer function (FTT; black line) obtained from the velocity profiles inversion and the empirical transfer function (FTE; red line) obtained from the spectral ratios for site IC-33.

with a jump that defines two tendencies. The average of the curves is between 2 and 20 Hz, with a moderate deflection at 8 Hz. These tendencies are associated with two frequency ranges corresponding to different vibration modes of the Rayleigh waves. Our results show that the velocities for *Curve 1* vary between 600 and 2000 m/s for frequencies between 0.6 and 1.0 Hz, whereas for *Curve 2* they vary between 170 and 800 m/s for frequencies between 2.0 and 15 Hz. Because of the complexity of the dispersion curve, we conducted testing to obtain phase velocities combining the fundamental and higher modes of the dispersion curve, according to Figure 4. We then inverted the data subsets to reconstruct

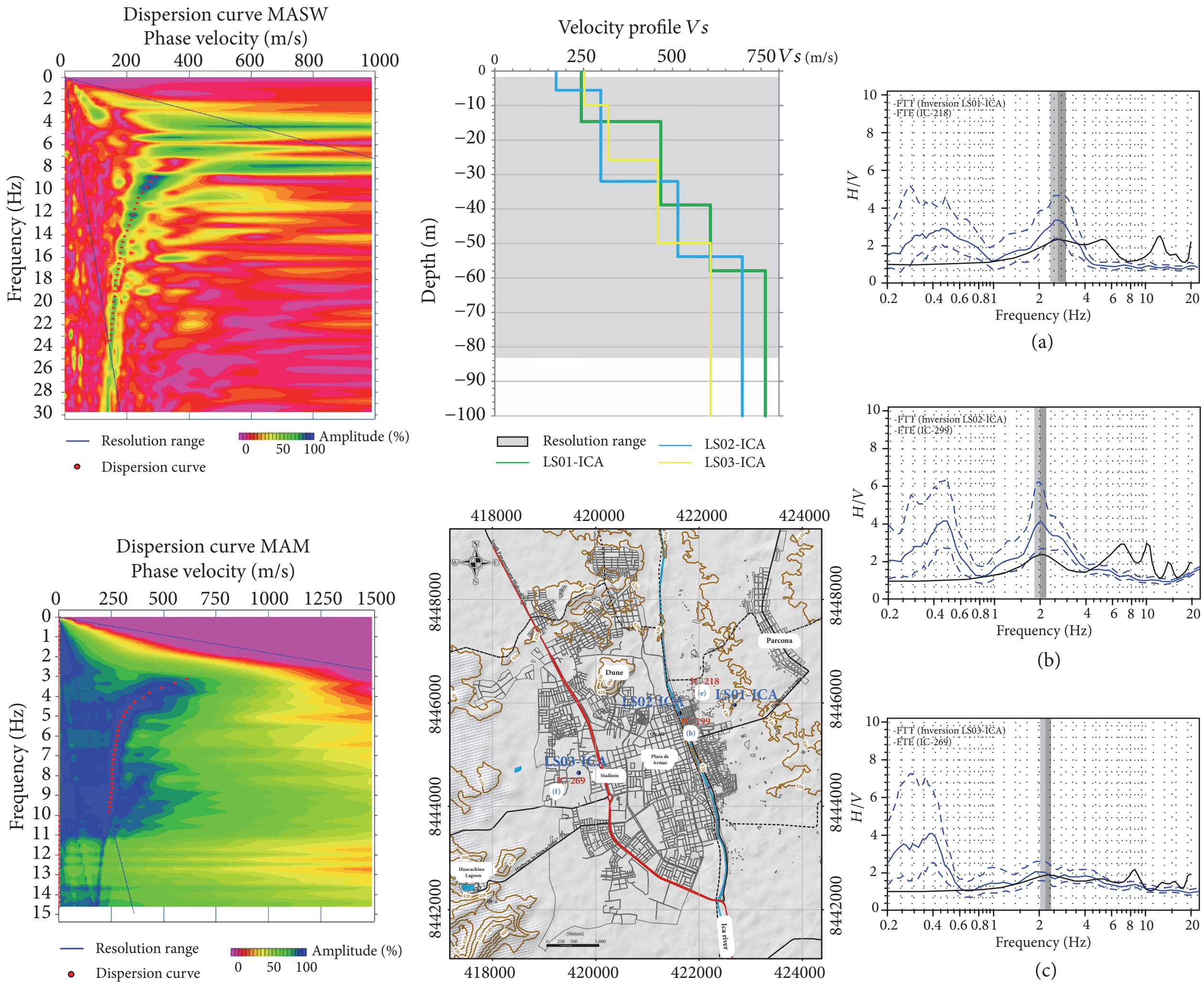

Figure 5: The left panels show the dispersion curves obtained with multichannel analysis of surface waves (MASW; top) and multichannel analysis of microtremors (MAM; bottom) methods. Here the averages and their inversions allow us to determine the velocity profile. The central plots show the velocity models (top) for the three linear arrays (bottom). The validation of the results is shown in the plots to the right. The inversion allowed us to obtain a theoretical transfer function (FTT; black line), which is superposed to the empirical transfer function (FTE; blue line) and shows a good correlation (degree of correspondence) with the fundamental frequency defined by the vertical gray line.

velocity profiles. We evaluated the effects of frequency range and combining of mode by comparing the inverted models obtained from the empirical transfer function (FTE) datasets (H/V: IC-33) with the theoretical transfer function (FTT) datasets theoretically obtained from the F-K method.

The results from four different tests are described thus: *Test 1:* Curve 1 corresponds to a fundamental mode of the Rayleigh waves and Curve 2 is subdivided into the first and second superior modes of the Rayleigh waves (2.1 and 2.2, resp.). *Test 2:* Curve 1 corresponds to a fundamental mode of the Rayleigh waves and Curve 2 corresponds to a first superior mode. *Test 3:* Curve 1 corresponds to a fundamental mode. *Test 4:* Curve 2 corresponds to a fundamental mode. For the first three tests, we obtain velocities lower than 180 m/s at 25 m and 300 m/s at 38 and 136 m, respectively. These results are not consistent with the geology, geomorphology, and stratigraphy of the study area; therefore, we consider these scenarios not representative of the area. Unlike these tests, Test 4 considers three shallow interfaces located at 4, 16, and 60 m. The first low-velocity layer would correspond to alluvial material and sandy soils, followed by the two layers showing velocities of 250 and 400 m/s, composed of moderately consolidated alluvial material to weakly compacted materials. Here as the depth increases, Vs increases above 900 m/s. In this last case, FTT and FTE coincide with the fundamental frequency of 1.8 Hz; thus, this result is consistent with the areas geology, geomorphology, and stratigraphy.

4.2.2. 1D Profile Using MASW and MAM. We performed MASW and MAM surveys on the borders and in the central part of the basin. The combination of MASW and MAM techniques allowed us to obtain velocity profiles at depths up to 60 and 100 m. The obtained results are consistent with a model consisting of three layers (Figure 5); the first with Vs between 170 and 180 m/s is composed of loose alluvial material (sandy soils); the second with *Vs* between 220 and 300 m/s is composed of moderately consolidated alluvial material; and the third with *Vs* between 400 and 460 m/s is composed of weakly compacted materials. It is important to note that as the depth of the layer increases *Vs* reaches values above 600 m/s. These *Vs* values correspond to layers 40 m thick to the east of the city and 60 m thick to the west. At greater depths, *Vs* increases to 800 to 900 m/s. In Figure 6 we present the results of the inversion, and we observe that for the fundamental frequency there is a correspondence between FTT and FTE represented by the gray line in each plot.

4.3. Depth of Soil-Rock Interface, Using Gravimetric Analysis. In Figure 7(a) we show the corrected Bouguer anomaly, which we obtained using the spectral analysis method proposed by Spector (1968) and Grant (1970). In Figure 7(b), we identify three gravimetric sources, associated with a residual or shallow anomaly (sources 1 and 2) and a regional or deeper (source 3) anomaly. In Figure 7(c), we present the gravimetric profile including our interpretation. To the west, we observe that the sedimentary layer is 150 m thick, decreasing to 60 m as the topographic elevation increases. These results provide evidence that the geomorphology of the Ica Basin's soil-rock interface is quite irregular because thicker sediment layers are on the basin's western border.

5. Discussions

The spectral ratio curves are useful for determining the soil responses; its resolution is related to the impedance contrast of the materials, allowing defining different frequencies and/or frequency ranges at specific sites [36]. In some cases, a single peak indicates a homogeneous soil, and in other cases, more peaks are consistent with heterogeneous soils. However these peaks may not be directly associated with soil stratigraphy, but rather with nonlinear effects that sometimes lead to inadequate interpretation [37]. Hence, it is important to carefully analyze each peak frequency.

The soils in Ica respond to two frequency ranges ($F0$: 0.4–0.8 Hz and $F1$: 1.0–3.0 Hz). Following the methodology of Semblat et al. (2002), the maximum relative amplifications are analyzed in terms of amplitude, frequency, and location to evaluate their correspondence with geomorphology. In the central part of Ica, $F0$ shows an amplification factor of four, which decreases rapidly toward the west and gradually toward the east (Parcona village). $F1$ shows amplification factors between two and three in the sites on the right margin of the Ica River and amplification factors of five on the left margin. We observe that these values increase rapidly toward Parcona village, which is 30 m higher with respect to the elevation of the river. In general, these results show a correspondence of $F0$ with regional sources that are modulated by the Ica Basin's geomorphology and a correspondence of $F1$ directly with the stratigraphy of the sediments deposited on the basin. The results using seismic methods allowed us to determine that the Ica Basin's shallow stratigraphic limit fluctuates between 50 and 60 m depth with *Vs* between 600 and 900 m/s. The gravimetric profiles also show that sediment thickness is variable along the profile, with layers of ~150 m to the west and 60 m to the east.

To determine the depth of the more representative interfaces, we applied the relation To = $4H/Vs$ [38], considering *Vs* values of 400 and 900 m/s, with an average frequency of 1.5 Hz. Using these parameters, we found two interfaces, one at a depth of 66 and one at 150 m. The first interface appears to correlate with moderately consolidated to slightly compacted alluvial materials, and the second appears to correlate with the soil-rock interface. These results agree with those obtained from gravity measurements. On the other hand, in Figure 7 we show the polynomial fit used to determine layer thickness, which we then used to construct the 2D model for the city of Ica. The results show that the basin consists of an irregular concave surface with depths of 60 and 150 m in the center of Ica, increasing rapidly to the west and decreasing gradually to the east.

Our results allow us to conclude that $F1$ corresponds to the fundamental frequency of Ica subsoil and $F0$ is harmonic with a regional origin [20] modulated by the Ica Basin. Finally, the frequency variations at depth that are associated with the physical characteristics of the soil, local topography, and geomorphology (dunes, small hills, and plateaus) allow us to characterize and infer the geometry and alluvial contents of Ica. The depth and irregularities of the basin generate seismic waves associated with resonance effects within layers of heterogeneous composition.

6. Conclusions

In this study we determined that the soils in the city of Ica respond to two frequency ranges: $F0$ (0.4–0.8 Hz) and $F1$ (1.0–3.0 Hz). $F0$ is associated with a regional source modulated by basin geomorphology and $F1$ is associated with a local source that corresponds to the dynamic response of the sediment layer.

Gravimetric and seismic analysis results show that the depth of the rock-soil interface under Ica varies from 150 m to the west to 60 m to the east. The 2D model suggests that the Ica Basin's geomorphology consists of a concave structure with depths that range from 120 to 150 m in the center and decrease rapidly to the west and gradually to the east.

The correlation of the results obtained using the seismic, geophysical, and geotechnical methods suggests that the Ica Basin's irregular geomorphology plays an important role in the dynamic response of Ica's soils to low frequencies, which produces a variation in the frequencies and relative amplification in soils despite a relatively flat surface topography. The structural damage associated with the 2007 Pisco earthquake was larger in the west, which can be explained by the thicker layer there and the variable dynamic behavior.

Conflicts of Interest

The authors declare that they have no conflicts of interest.

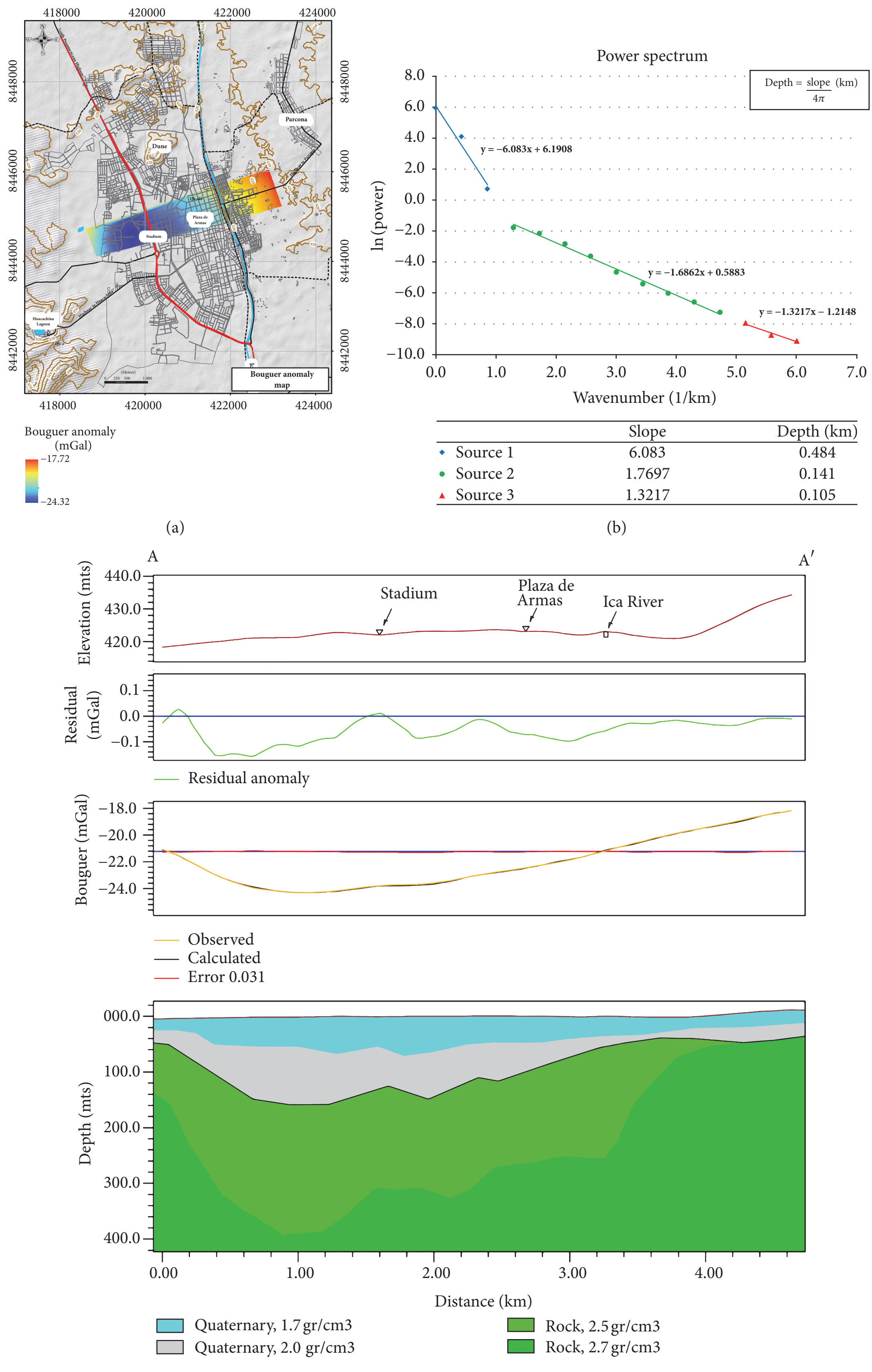

FIGURE 6: (a) Bouguer gravity anomaly map; (b) spectral analysis derived from the Bouguer gravity anomaly; and (c) gravimetric profile A-A′ (see Figure 1) showing sedimentary deposits and the rocky basement.

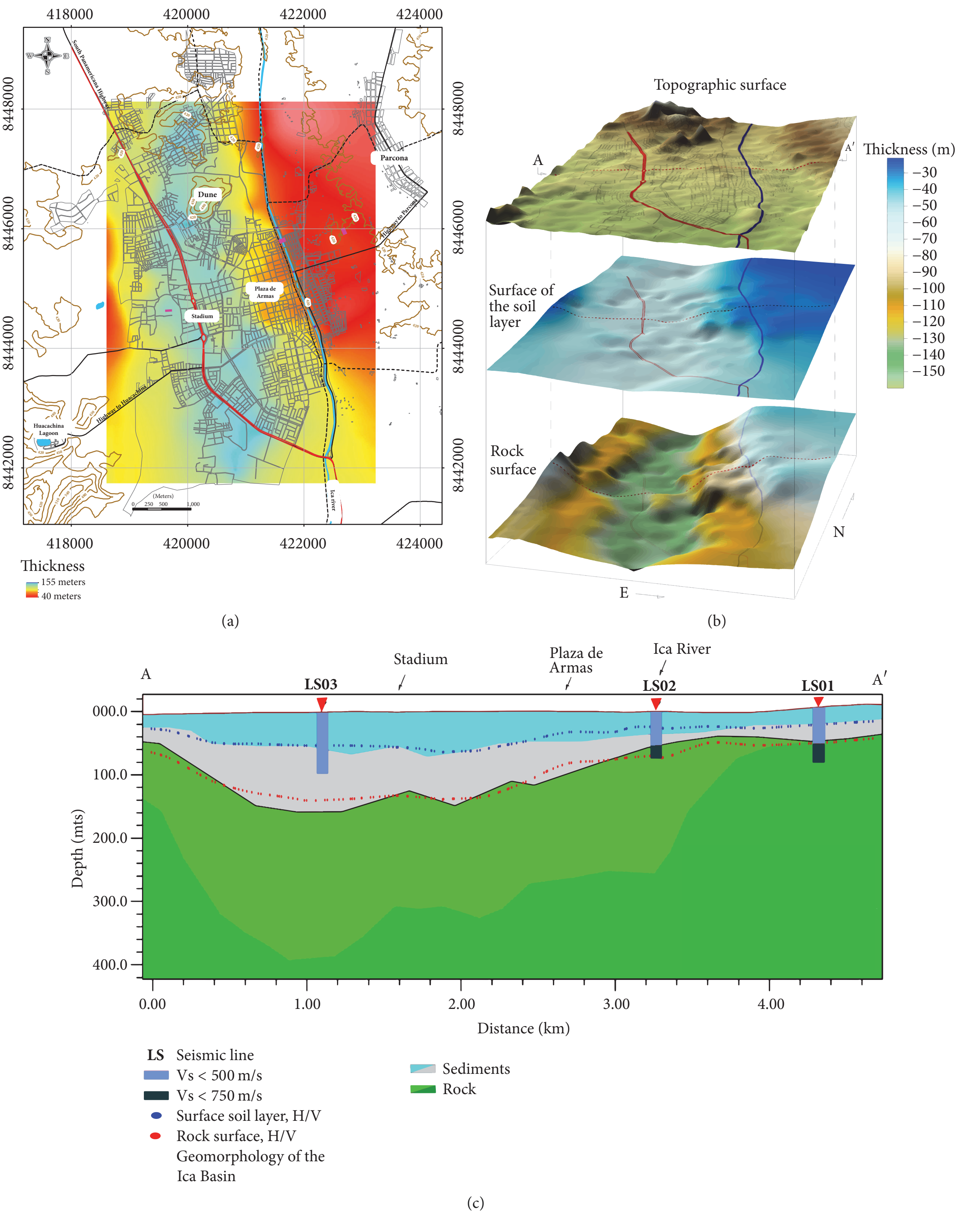

Figure 7: (a) Contour depth map derived from the predominant frequencies; (b) 3D schema of the Ica Basin; and (c) cross section of the Ica Basin (A-A′), superposed on the results obtained using seismic and gravimetric methods.

Acknowledgments

This research was supported by Geophysical Institute of Peru (IGP). The authors would like to thank Betrand Guillier and Marc Wathelet of the "Institut de Recherche pour le Developpement (IRD)," for training on the use of tool of Geopsy and their valuable contributions to the manuscript. Also thanks are due to Hugo Perfettini (IRD) for the support, advice, and contribution to their professional life.

References

[1] H. Tavera and I. Bernal, "The pisco (Peru) earthquake of 15 August 2007," *Seismological Research Letters*, vol. 79, no. 4, pp. 510–515, 2008.

[2] INDECI, *Reporte del sismo del*, Instituto Nacional de Defensa Civil, 2007.

[3] H. Tavera, I. Bernal, F. Stresser, M. Arango-Gavina, J. Alarcon, and J. Bommer, "Ground Motions observed during the 15 August 2007 Pisco, Peru, event," *Bulletin of Earthquake Eingineering*, 2008.

[4] W. León and V. Torres, "Mapa geológico actualizado del cuadrángulo de Ica (29 - i)," *INGEMMET, DGR*, 2001.

[5] S. Bonnefoy-Claudet, S. Baize, L. F. Bonilla et al., "Site effect evaluation in the basin of Santiago de Chile using ambient noise measurements," *Geophysical Journal International*, vol. 176, no. 3, pp. 925–937, 2009.

[6] J. C. Gomez, S. Ortiz, and C. Chiroque, *Informe técnico, Geología y geotecnia de la ciudad de Ica*, 2013.

[7] K. Kanai and T. Tanaka, "On microtremors. VIII," *Bulletin of the Earthquake Research Institute Tokyo University*, vol. 39, pp. 97–114, 1961.

[8] M. Nogoshi and T. Igarashi, "On the amplitude characteristics of microtremor (part 2)," *Journal of the Seismological Society of Japan*, vol. 24, pp. 26–40, 1971.

[9] Y. Nakamura, "Method for dynamic characteristics estimation of subsurface using microtremor on the ground surface," *Quarterly Report of RTRI (Railway Technical Research Institute) (Japan)*, vol. 30, no. 1, pp. 25–33, 1989.

[10] H. Okada, "The microtremors survey method, Geophysical Monograph Series 12," *Society of Exploration Geophysics of Japan*, p. 155, 2004.

[11] Y. Nakamura, "Clear Identification of Fundamental Idea of Nakamura's Technique and its applications in the hill zone of México City," *Bulletin of the Seismological Society of America*, vol. 82, pp. 24–43, 2000.

[12] J. Lermo and F. J. Chavez-García, "Site effect evaluation using spectral ratios with only one station," *Bulletin of the Seismological Society of America*, vol. 83, pp. 1574–1594, 1993.

[13] F. Leyton, S. Sepulveda, M. Astroza et al., "Zonificación sísmica de la cuenca de Santiago," in *Congreso Chileno de Sismología e Ingeniería Antisφsmica, X Jornadas*, pp. 22–27, Chile, 2010.

[14] R. Lacoss, E. Kelly, and M. Toksöz, "Estimation of seismic noise structure using arrays," *Geophysics*, vol. 34, no. 1, pp. 21–38, 1969.

[15] T. Kvaerna and F. Ringdahl, "Stability of various fk estimation techniques, Norsar semiannual technical summary," Tech. Rep., 1, –86, 1986.

[16] S. Foti, R. Lancellota, L. V. Socco, and L. Sambuelli, "Application of FK analysis of surface waves for geotechnical characterization," in *Proceedings of the Proc. 4th International Conference on Recent Advances in Geotechnical Earthquake Engineering and Soil Dynamics, Paper No. 1.14*, San Diego, California, 2001.

[17] K. Tokimatsu, Y. Miyadera, and S. Kuwayama, "Determination of Shear Wave Velocity Structures from Spectrum Analyses of Short-Period Microtremors," in *Proceedings of the 10th World Conf. on Earthquake Eng*, vol. 1, pp. 253–258, 1992.

[18] D. J. Zywicki, *Advanced Signal Processing Methods Applied to Engineering Analysis of Seismic Surface Waves*, 1999.

[19] K. Aki and P. G. Richards, *Quantitative Seismology*, University Science Books, 2002.

[20] K. Aki and P. Richards, *Quantitative Seismology: Theory and Methods*, New York, 1980.

[21] M. Wathelet, *Array recordings of ambient vibrations: surface-wave inversion*, Liège University, Belgium, 2005a.

[22] M. Wathelet, *Geopsy geophysical signal database for noise array processing*, Software, LGIT, Grenoble, France, 2005b.

[23] M. Wathelet, "An improved neighborhood algorithm: Parameter conditions and dynamic scaling," *Geophysical Research Letters*, vol. 35, no. 9, Article ID L09301, 2008.

[24] D. Fäh, G. Stamm, and H. Havenith, "Analysis of three-component ambient vibration array measurements," *Geophysical Journal International*, vol. 172, pp. 199–213, 2008.

[25] K. Aki, "Space and time spectra of stationary stochastic waves, with special reference to microtremors," *Bull, Earthquake Res. Inst. Tokyo Univ*, vol. 35, pp. 415–456 (1 plate), 1957.

[26] J. Xia, R. D. Miller, and C. B. Park, "Estimation of near-surface shear-wave velocity by inversion of Rayleigh waves," *Geophysics*, vol. 64, no. 3, pp. 691–700, 1999.

[27] S. Foti, L. Sambuelli, L. V. Socco, and C. Strobbia, "Experiments of joint acquisition of seismic refraction and surface wave data," *Near Surface Geophysics*, vol. 1, pp. 119–129, 2003.

[28] M. Wathelet, D. Jongmans, M. Ohrnberger, and S. Bonnefoy-Claudet, "Array performance for ambient vibrations on a shallow structure and consequences over vs inversion," *Journal of Seismology*, vol. 12, pp. 1–19, 2008.

[29] M. Wathelet, D. Jongmans, and M. Ohrnberger, "Surface-wave inversion using a direct search algorithm and its application to ambient vibration measurements," *Near Surf Geophys*, vol. 2, pp. 211–221, 2004.

[30] F. J. Sánchez-Sesma, V. J. Palencia, and F. Luzón, "Estimation of local site effects during earthquakes: an overview," *ISET Journal of Earthquake Technology*, vol. 39, no. 3, pp. 167–193, 2002.

[31] C. B. Park, R. D. Miller, and J. Xia, "Multichannel analysis of surface waves," *Geophysics*, vol. 64, no. 3, pp. 800–808, 1999.

[32] C. B. Park and R. D. Miller, "Roadside passive multichannel analysis of surface waves (MASW)," *Journal of Environmental & Engineering Geophysics*, vol. 13, no. 1, pp. 1–11, 2008.

[33] W. Hinze, "New standards for reducing gravity data, The North American gravity database," *Geophysics*, vol. 70, no. 4, pp. 25–32, 2005.

[34] M. F. Kane, "A Comprehensive System of Terrain Corrections Using a Digital Computer," *Geophysics*, vol. 27, no. 4, pp. 455–462, 1962.

[35] D. Nagy, "The gravitational attraction of a right rectangular prism," *Geophysics*, vol. 31, no. 2, pp. 362–371, 1966.

[36] M. Pilz, S. Parolai, M. Picozzi et al., "Shear wave velocity model of the Santiago de Chile basin derived from ambient noise measurements: A comparison of proxies for seismic site conditions and amplification," *Geophysical Journal International*, vol. 182, no. 1, pp. 355–367, 2010.

[37] C. Cornou, P. Guéguen, P.-Y. Bard, and E. Haghshenas, "Ambient noise energy bursts observation and modeling: Trapping of harmonic structure-soil induced-waves in a topmost sedimentary layer," *Journal of Seismology*, vol. 8, no. 4, pp. 507–524, 2004.

[38] SESAME-Project EVG1-CT-2000-00026, "Deliverable D19.06," 2009, http://sesame-fp5.obs.ujf-grenoble.fr/Deliverables/Del-D19-Wp06.pdf.